Article

Discovery Medicine 2026; 38(205): 453–467
https://doi.org/10.24976/Discov.Med.202638205.38

C-X-C Motif Chemokine Ligand 8: A Promising Prognostic Biomarker for HPV 16-Driven Cervical Cancer

Yan Li[1], Huiying Li[1], Li Shi[2], Ying Cui[1,*]

[1]Department of Obstetrics and Gynecology, Hongqi Hospital Affiliated to Mudanjiang Medical University, 157000 Mudanjiang, Heilongjiang, China
[2]Pathology Diagnostic Center, Hongqi Hospital Affiliated to Mudanjiang Medical University, 157000 Mudanjiang, Heilongjiang, China
*Correspondence: mdjhqyycuiying@163.com (Ying Cui)

Submitted: 30 September 2025 Revised: 16 December 2025 Accepted: 31 December 2025 Published: 20 February 2026

Background: The persistent expression of high-risk human papillomavirus (hrHPV) E6 oncoproteins is a critical determinant in driving and maintaining the malignant phenotype of cervical cancer, a pathogenic process where autophagy serves as a key regulatory mechanism. This study aimed to identify autophagy-related genes as potential biomarkers for prognostic evaluation in cervical cancer.

Methods: This study established an HPV 16 E6-induced C33a cervical cancer cell model, which was treated with the autophagy activator rapamycin or inhibitor 3-methyladenine to modulate autophagy. The expression of the autophagy-related gene C-X-C motif chemokine ligand 8 (CXCL8) was analyzed by reverse transcription-quantitative PCR (RT-qPCR), western blotting, and enzyme-linked immunosorbent assay. Cell viability, migration, invasion, and apoptosis were assessed using the Cell Counting Kit-8 assay, wound healing assay, Transwell assay, and Terminal deoxynucleotidyl transferase–mediated deoxyuridine triphosphate nick-end labeling (TUNEL) assays, respectively. Furthermore, CXCL8 expression levels in tumor tissues from cervical cancer patients with favorable (n = 81) and unfavorable (n = 61) prognosis were examined by immunohistochemistry and RT-qPCR. Univariate and multivariate Cox proportional hazards regression analyses were conducted to identify independent risk factors influencing disease-free survival (DFS) in cervical cancer patients. Receiver operating characteristic (ROC) curve analysis was employed to evaluate the predictive value of CXCL8 for unfavorable prognosis risk.

Results: Mechanistic studies indicated the participation of CXCL8 in HPV 16 E6–induced malignant phenotypes. The autophagy activator rapamycin or CXCL8-neutralizing antibody could neutralize the oncogenic effects of HPV 16 E6. CXCL8 was highly expressed in tumor tissues with poor prognosis. It showed correlations with poor tumor differentiation, cervical infiltration depth $\geq$2/3, and lymph node metastasis, independent of clinical stage. CXCL8 was identified as an independent prognostic factor in cervical cancer [hazard ratio = 3.143, 95% confidence interval (CI): 1.519–6.507, p = 0.002] and was significantly correlated with inferior DFS (χ^2 = 34.905, $p < 0.0001$). Furthermore, a model combining CXCL8 with squamous cell carcinoma antigen and cytokeratin 19 fragment showed promising prognostic accuracy, achieving an area under the curve of 0.897 (95% CI: 0.835–0.942) with 90.16% sensitivity and 88.89% specificity.

Conclusion: The *CXCL8* gene promotes cervical cancer progression by contributing to the regulation of autophagy mediated by HPV 16 E6. This functional role underpins its potential utility as a clinical prognostic biomarker.

Keywords: cervical cancer; prognosis; C-X-C motif chemokine ligand 8; autophagy; biomarker

Introduction

Cervical cancer constitutes a major global health burden among gynecological malignancies, accounting for an estimated 661,000 new diagnoses and 348,000 fatalities each year [1]. Despite considerable progress in treatment modalities, the prognosis for patients diagnosed with advanced-stage cervical cancer remains dismal. Current treatment strategies and prognostic assessment primarily rely on clinical staging and pathological characteristics. Several key clinicopathological factors have been identified as determinants of recurrence and prognosis in cervical cancer, including histological subtype, International Federation of Gynecology and Obstetrics (FIGO) stage, lymph node metastasis, and tumor size. However, patients at the same clinical stage do not always experience identical outcomes. Considerable controversy persists regarding certain prognostic factors such as patient age, pathological type, and tumor differentiation [2,3]. Complementing established prognostic parameters, a growing body of evidence has identified multiple novel biomarkers that show significant correlations with survival outcomes in cervical cancer patients [4,5]. Therefore, some studies have focused on developing precise prognostic tools for the early identification of high-risk patients susceptible to treatment failure.

Molecular oncology has identified that human oncogenic viruses, including high-risk human papillomavirus (hrHPV), Epstein–Barr virus, hepatitis B virus, hepatitis C virus, Kaposi's sarcoma–associated herpesvirus, and human T-lymphotropic virus 1, contribute to carcinogenesis by promoting chronic inflammation, uncontrolled proliferation, and malignant transformation [6,7]. The development of invasive cervical carcinoma is causally linked to infection with hrHPV genotypes, most notably HPV 16 and 18 [8]. The persistent expression of E6/E7 oncoproteins exerts carcinogenic effects by interacting with cellular protein functions, thereby promoting tumor proliferation, migration, and invasion, and concurrently inhibiting apoptosis and enabling immune evasion [9,10]. In cervical cancer, increased expression of the E6 oncogene and the E6* isoform correlates with a marked reduction in overall survival (OS), identifying a patient subgroup with an unfavorable prognosis [11]. Viral oncoproteins are essential for sustaining the malignant phenotypes. Current studies have attempted to discover novel hrHPV-associated biomarkers. Autophagy plays a central role in the pathogenesis of diverse solid tumors by modulating viral replication and facilitating immune evasion [12]. This process is directly targeted by viral oncoproteins, such as hepatitis B virus X protein, hepatitis C virus nonstructural protein 4B/nonstructural protein 5A, and the Epstein-Barr virus replication and transcription activator [13,14]. The role of hrHPV in driving malignant transformation and promoting aggressive tumor phenotypes is well established. However, its multifaceted interactions with cellular homeostasis mechanisms, particularly through autophagy modulation, remain poorly elucidated. Emerging evidences reveal paradoxical autophagic effects in HPV pathogenesis. For instance, HPV 16 achieves autophagy suppression through activating the phosphatidylinositol 3-Kinase (PI3K)/Ak transforming (Akt)/mammalian target of rapamycin (mTOR) signaling axis, a strategy that thereby potentiates its infectivity [15]. HPV 16 E7 induces autophagic flux in keratinocytes, while concomitantly increasing cellular susceptibility to serum starvation-induced death [16]; the superior therapeutic response observed in HPV-positive oropharyngeal squamous cell carcinoma, relative to its HPV-negative counterpart, may be linked to the dysregulation of critical autophagy-related genes (ARGs) [17]. However, the prognostic implications of autophagy in hrHPV-induced cervical carcinogenesis still need to be elucidated.

Autophagy dysregulation is a well-established co-carcinogenic factor in hrHPV infection, making the analysis of ARGs a promising approach for identifying prognostic biomarkers in cervical cancer. The proinflammatory chemokine C-X-C motif chemokine ligand 8 (CXCL8, also known as interleukin-8—the first identified chemokine), which is implicated in various malignancies, has been shown to promote tumor migration through autophagy suppression [18]. However, the specific role and regulatory mechanism of CXCL8 in hrHPV-driven cervical cancer, particularly in relation to key oncoproteins such as HPV 16 E6—known for its role in immune evasion and cellular transformation—remain unclear. Therefore, this study aims to elucidate how CXCL8 modulates autophagy in hrHPV-positive cervical cancer cells and to establish a causal link between CXCL8 expression and autophagic activity. Our findings are expected to provide a theoretical basis for considering CXCL8 as a potential prognostic biomarker and therapeutic target in hrHPV-associated cervical carcinogenesis.

Methods

Patients and Clinical Samples

This retrospective cohort study received ethical approval from the Ethics Committees of Hongqi Hospital Affiliated to Mudanjiang Medical University (Approval No. 202028) and was conducted in compliance with the Declaration of Helsinki. This retrospective study analyzed 142 patients with histologically confirmed cervical cancer admitted between January 2020 and July 2022. Based on the occurrence of a three-year disease-free survival (DFS) event, patients were stratified into two groups: a favorable prognosis group ($n = 81$), in which no DFS event occurred, and an unfavorable prognosis group ($n = 61$), which experienced DFS events. Written informed consent was procured from all participants prior to the collection of preoperative serum and postoperative tissue specimens. Patient eligibility was defined by the following criteria: (1) patients with a histologically confirmed diagnosis of cervical cancer; (2) availability of complete clinical and follow-up records; and (3) patients who had undergone radical hysterectomy as primary treatment. The study exclusion criteria were defined as follows: (1) patients with synchronous primary malignancies in other systems; (2) patients with cardiac, hepatic, or renal dysfunction; (3) patients with anticipated survival of less than 6 months; and (4) patients with confirmed distant metastasis prior to surgery.

Patient Follow-Up

Postoperative follow-up was conducted through medical record reviews and telephone interviews every 3 months for 3 years, continuing until August 30, 2025. The collected data encompassed routine diagnostic imaging (computed tomography, magnetic resonance imaging, and bone scans) and laboratory findings. Follow-up records comprised detailed documentation of disease progression, recurrence, metastasis, survival status, and the final follow-up date. Based on the occurrence of a three-year DFS event, patients were stratified into two prognostic groups: (1) the favorable prognosis group (no DFS event), comprising patients who remained clinically stable with no evidence of disease recurrence, distant metastasis, or mortality during follow-up; and (2) the poor prognosis group (DFS event oc-

curred), which included patients who experienced disease progression, locoregional recurrence, metastatic dissemination, or cancer-related death [19,20].

Grouping

The prognostic value of serum CXCL8 levels was evaluated using receiver operating characteristic (ROC) curve analysis. With the 3-year follow-up outcomes (unfavorable prognosis = 1, favorable prognosis = 0) as the state variable and baseline CXCL8 levels as the test variable, the optimal cutoff value was determined to be 43.6 pg/mL by maximizing the Youden index. Accordingly, patients were stratified into a high-CXCL8 group ($\geq$43.6 pg/mL, n = 73) and a low-CXCL8 group ($<$43.6 pg/mL, n = 69).

Treatment Strategies for Cervical Cancer

For early-stage patients (FIGO I–IIA) with favorable prognoses, radical surgery serves as the cornerstone. Procedure selection depends on staging and fertility needs: cervical conization for stage IA1 with fertility preservation requirements, or radical hysterectomy for stages IA2-IIA. Postoperative radiotherapy is indicated when high-risk factors such as lymph node metastasis or positive margins are present. For patients with poor prognoses, including those with locally advanced (FIGO IB3-IVA), metastatic, or special pathological types, concurrent chemoradiotherapy remains the standard for locally advanced disease, with pembrolizumab immunotherapy recommended for stages III-IVA. For recurrent or metastatic disease, systemic therapy predominates, incorporating PD-1 inhibitors, the anti-angiogenic agent bevacizumab, and antibody-drug conjugates such as Tisotumab Vedotin. All therapeutic decisions should be individualized based on FIGO stage, pathological type, biomarker profiles, and patient-specific circumstances [21].

Bioinformatics Analyses

CXCL8 expression data in cervical cancer were sourced from publicly accessible databases, including The Cancer Genome Atlas (http://portal.gdc.cancer.gov) and the Gene Expression Profiling Interactive Analysis (GEPIA) platform (http://gepia.cancer-pku.cn/). Subsequently, the association between CXCL8 expression and patient OS as well as DFS was evaluated using the Kaplan-Meier plotter (http://kmplot.com/analysis), with statistical significance determined by the log-rank test. It is noteworthy that when integrating data, the GEPIA platform requires samples to have both expression and survival information for Kaplan-Meier analysis, whereas box plots require only expression data. This difference in criteria results in a slight discrepancy in the number of samples included between the two analyses (survival analysis n = 304, box plots analysis n = 306).

Cell Culture

C33a cells were acquired from the Chinese Academy of Medical Sciences (Beijing, China) and maintained in Dulbecco's modified Eagle's medium (DMEM; Gibco, NY, USA, Cat. No. 11880028) containing 10% fetal bovine serum (FBS; Gibco, Cat. No. 16000044), along with penicillin (100 IU/mL) and streptomycin (100 µg/mL) (Gibco, Cat. No. 15140122). The cells were cultured at 37 °C in a humidified incubator with 5% CO_2. The C33a cell line was tested and confirmed negative for mycoplasma contamination. The genetic integrity was monitored annually via three complementary approaches: short tandem repeat authentication, quantification of population doubling times, and systematic morphological evaluation.

Plasmids Construction and Transfection

The full-length human CXCL8 cDNA was cloned into the pcDNA3.1 vector (Invitrogen, CA, USA, Cat. No. 11510866) via BamHI and XhoI restriction sites to generate the pcDNA3.1-CXCL8 (pc-CXCL8) plasmid. The cDNA was amplified using the following primers: sense, 5′-AGT GCT AAA GAA CTT AGA TGT CAG-3′ and antisense, 5′-TCA TGA ATT CTC AGC CCT CTT CAA AAA-3′. The primers used for constructing the pcDNA3.1-HPV 16 E6 plasmid were: sense, 5′-ATG CAC CAA AAG AGA ACT GC-3′ and antisense, 5′-TCA TTA CAG CTG GGT TTC TCT ACG TG-3′. An empty pcDNA3.1 vector (pc-NC) served as a negative control; the primers: sense, 5′-CTA GAG AAC CCA CTG CTT AC-3′ and antisense, 5′-TAG AAG GCA CAG TCG AGG-3′. Transfection of C33a cells was performed using Lipofectamine 2000 (Invitrogen, Cat. No. 11668027) following the manufacturer's protocol. The cells were transfected with one of the following plasmids at a concentration of 2.5 µg/mL: pc-CXCL8, pc-NC, or the HPV 16 E6 vector.

Treatment With Autophagy Modulators and Exogenous Anti-CXCL8 Antibody

C33a cells were subjected to various treatments to modulate autophagy and inhibit CXCL8 signaling. Specifically, autophagy was inhibited by adding 10 mM 3-methyladenine [22] (3-MA; Chunshi, Shanghai, China, Cat. No. CS-01Y63520) directly to the culture medium. Conversely, autophagy was activated by treating cells with 3 µM rapamycin [22] (Rapa; Chunshi, Cat. No. CS-C6951), which was initially dissolved in dimethyl sulfoxide (DMSO; Chunshi, Cat. No. CS-01F97073) and then diluted in the medium. A vehicle control, consisting of medium supplemented with 0.1% DMSO, was established in parallel. Additionally, a neutralizing anti-CXCL8 antibody was administered directly into the culture medium at a final concentration of 350 ng/mL. Untreated cells were maintained as a baseline control for all experimental groups.

Reverse Transcription–Quantitative Polymerase Chain Reaction (RT-qPCR)

Total RNA was isolated from cells with TRIzol reagent (Sigma-Aldrich, St. Louis, MO, USA, Cat. No. 93289) per the manufacturer's protocol. Following extraction, RNA quality was confirmed on a NanoDrop One spectrophotometer (Thermo Fisher, Waltham, MA, USA, Cat. No. 840317400), ensuring all samples had an A260/A280 ratio exceeding 1.8. Subsequent reverse transcription was carried out with the HiScript III All-in-one RT SuperMix (Vazyme, Nanjing, Jiangsu, China, Cat. No. R333-01), followed by quantitative PCR using SYBR Green Master Mix (Vazyme, Cat. No. Q311-02). The primer sequences employed are listed below: C-X-C motif chemokine ligand 10 (*CXCL10*): (forward) 5′-GTG GCA TTC AAG GAG TAC CTC-3′, (reverse) 5′-TGA TGG CCT TCG ATT CTG GAT T-3′; C-X-C motif chemokine ligand 12 (*CXCL12*): (forward) 5′-TGT GAC GGC AGG GAA ATG TA-3′, (reverse) 5′-TCT GCT CTA ACA CAG AGG GAA AC-3′; C-X-C motif chemokine ligand 5 (*CXCL5*): (forward) 5′-AGC TGC GTT GCG TTT GTT TAC-3′, (reverse) 5′-TGG CGA ACA CTT GCA GAT TAC-3′; C-X-C motif chemokine ligand 1 (*CXCL1*): (forward) 5′-AAC ATG CCA GCC ACT GTG AT-3′, (reverse) 5′-GCC CCT TTG TTC TAA GCC AG-3′; *CXCL8*: (forward) 5′-ACT GAG AGT GAT TGA GAG TGG AC-3′, (reverse) 5′-AAC CCT CTG CAC CCA GTT TTC-3′; C-X-C motif chemokine ligand 16 (*CXCL16*): (forward) 5′-CCC GCC ATC GGT TCA GTT C-3′, (reverse) 5′-CCC CGA GTA AGC ATG TCC AC-3′; C-C motif chemokine ligand 19 (*CCL19*): (forward) 5′-TAC ATC GTG AGG AAC TTC CAC T-3′, (reverse) 5′-CTG GAT GAT GCG TTC TAC CCA-3′; C-X-C motif chemokine ligand 2 (*CXCL2*): (forward) 5′-GCT TGT CTC AAC CCC GCA TC-3′, (reverse) 5′-TGG ATT TGC CAT TTT TCA GCA TCT T-3′; C-X-C motif chemokine ligand 4 (*CXCL4*): (forward) 5′-ACT AGC TGC CTA CGT GTG TG-3′, (reverse) 5′-GCA TAA CCA GTA TTC ACA CCT TCC-3′; C-C motif chemokine ligand 5 (*CCL5*): (forward) 5′-CAG TCG TCC ACA GGT CAA GG-3′, (reverse) 5′-TCT TCT CTG GGT TGG CAC AC-3′; and glyceraldehyde-3-phosphate dehydrogenase (*GAPDH*): (forward) 5′-GGA GCG AGA TCC CTC CAA AAT-3′, (reverse) 5′-GGC TGT TGT CAT ACT TCT CAT GG-3′. The relative quantification of mRNA expression was determined through the $2^{-\Delta\Delta Ct}$ method [23].

Immunoblotting

Cellular proteins were extracted with lysis buffer, and equal amounts (40 µg per lane) were subjected to sodium dodecyl sulfate-polyacrylamide gel electrophoresis followed by transfer to polyvinylidene difluoride membranes (Merck Millipore, Burlington, MA, USA, Cat. No. IPVH00010). After blocking with 5% skimmed milk, the membranes were incubated overnight at 4 °C with primary antibodies against microtubule-associated protein 1A/1B-light chain 3 (LC3, 1:2000; Abcam, Waltham, MA, USA, Cat. No. ab192890) and CXCL8 (1:1000; Abcam, Cat. No. ab289967, Clone EPR26511-74). Following washes, the membranes were incubated with a horseradish peroxidase (HRP)-conjugated secondary antibody (1:3000; Abcam, Cat. No. ab6721) for 2 h at room temperature. Protein bands were visualized using an enhanced chemiluminescence kit (Cell Signaling Technology, Danvers, MA, USA, Cat. No. 6883) and quantified by densitometry with ImageJ software (National Institutes of Health, MD, USA, v1.54f).

Cell Viability Assay

Cell viability of C33a cells was assessed with the Cell Counting Kit-8 (CCK-8; Dojindo, Kumamoto, Japan, Cat. No. CK04). Briefly, cells were plated in 96-well plates at 10×10^3 cells/mL, subjected to experimental treatments for 48 h, and then incubated with 10 µL of CCK-8 solution per well for 4 h. Absorbance at 450 nm was recorded using a BioTek Synergy H1 microplate reader (BioTek Instruments, Model H1MF).

Wound Healing Assay

For the wound healing assay, cells were grown in six-well plates to 80–90% confluence. A standardized scratch wound was created with a sterile pipette tip (recorded as 0 h). After washing with phosphate-buffered saline, cells were cultured in complete medium for 48 h at 37 °C with 5% CO_2. Migration was documented by capturing four random microscopic fields per well at 200× magnification (Olympus BX53, Serial No.: 5D45165, Olympus Corporation, Tokyo, Japan). The relative migration distance was determined by applying the formula: Percentage of wound closure (%) = 100 × (A – B) / A, wherein A represents the initial wound width (at 0 h) and B represents the residual wound width after the incubation period (at 48 h) [24].

Cell Invasion Assay

Cell invasion was assessed using Matrigel-coated Transwell chambers (Millipore, Cat. No. CLS3422). Serum-starved cells were plated in the upper chamber at 5×10^5 cells/mL, with 10% FBS-DMEM as a chemoattractant in the lower chamber. After 48 h of incubation, non-invading cells were removed from the upper surface. Migrated cells on the lower membrane were fixed in 70% methanol, stained with 2% crystal violet (Maokang, Shanghai, China, Cat. No. MS4005-100G), and quantified under an Olympus BX53 microscope at 200× magnification.

Terminal Deoxynucleotidyl Transferase–Mediated Deoxyuridine Triphosphate Nick-End Labeling (TUNEL) Analysis

Apoptosis was assessed using the DeadEnd TUNEL system (Promega Corporation, WI, USA, Cat. No. G3250) according to the manufacturer's instructions. C33a cells

Table 1. Correlation between CXCL8 expression and clinicopathological characteristics in cervical cancer.

Pathological characteristics	CXCL8		χ^2	p
	Low (<43.6, n = 69)	High (≥43.6, n = 73)		
Age			0.001	0.973
≤50 years	31 (48.4)	33 (51.6)		
>50 years	38 (48.7)	40 (51.3)		
Tumor diameter			2.234	0.135
≤4 cm	37 (55.2)	30 (44.8)		
>4 cm	32 (42.7)	43 (57.3)		
FIGO staging			0.297	0.586
I∼II	40 (50.6)	39 (49.4)		
III	29 (46.0)	34 (54.0)		
Differentiation			4.235	0.040
Low	25 (39.1)	39 (60.9)		
Medium/high	44 (56.4)	34 (43.6)		
Cervical infiltration Depth			4.675	0.031
≥2/3	31 (40.3)	46 (59.7)		
<2/3	38 (58.5)	27 (41.5)		
Lymph node metastases			4.461	0.035
Yes	22 (37.9)	36 (62.1)		
No	47 (56.0)	37 (44.0)		

CXCL8, C-X-C motif chemokine ligand 8; FIGO, International Federation of Gynecology and Obstetrics.

were fixed, permeabilized, and incubated with the TUNEL reaction mixture. After washing, nuclei were counterstained with 4′,6-diamidino-2-phenylindole (DAPI, 1:2000 dilution; Beyotime Biotechnology, Shanghai, China, Cat. No. C1002), and slides were mounted for fluorescence microscopy (Olympus Corporation, Model BX53). Positive TUNEL ratio = (All TUNEL positive nuclei/All DAPI positive nuclei) × 100% [25].

Immunohistochemistry (IHC)

For IHC analysis, paraffin-embedded tissue sections underwent baking, deparaffinization, and rehydration followed by antigen retrieval. After blocking, sections were incubated with anti-CXCL8 primary antibody (1:100 dilution; Cell Signaling Technology, Cat. No. 94407; Clone E5F5Q) at 4 °C overnight, then with HRP-conjugated secondary antibody (1:1000; Abcam, Cat. No. ab6721) for 2 h at ambient temperature. Signal was developed using 3,3′-diaminobenzidine (DAB; Abcam, Cat. No. ab64238), and nuclei were counterstained with hematoxylin. Stained sections were visualized under an Olympus BX53 microscope, and a composite IHC score (range: 0–12) was derived by multiplying the staining intensity grade (0: negative; 1+: weak; 2+: moderate; 3+: strong) by the proportion of immunoreactive cells (0: <5%; 1+: 5–25%; 2+: 26–50%; 3+: 51–75%; 4+: >75%) [25].

Immunofluorescence Staining

Cells grown on glass coverslips were fixed with 4% paraformaldehyde, permeabilized with 0.1% Triton X-100, and blocked with 5% bovine serum albumin. Specimens were then incubated with anti-LC3 primary antibody (1:100 dilution; Abcam, Cat. No. ab181147) followed by fluorescein isothiocyanate (FITC)-conjugated secondary antibody (1:200 dilution; ProteinTech Group, IL, USA, Cat. No. SA00003-2). After nuclear counterstaining with DAPI (Beyotime; Cat. No. C1002), images were acquired using a confocal microscope (Model BX53, Serial No.: 5D45165, Olympus Corporation) and analyzed with ImageJ software (v1.54f; National Institutes of Health).

Enzyme-Linked Immunosorbent Assay (ELISA)

CXCL8 levels in serum and cell culture supernatants were quantified using commercial ELISA kits (R&D Systems, Minneapolis, MN, USA, Cat. No. DY208) according to the manufacturer's protocols. The obtained values were normalized against the total protein concentration.

Statistical Analysis

Data are expressed as mean ± standard deviation. Intergroup comparisons utilized Student's t-test (two groups) or one-way Analysis of Variance (ANOVA) with Tukey's post-hoc test (≥3 groups). Categorical variables in Table 1 were analyzed by chi-square test. Prognostic performance of CXCL8 was assessed by ROC curve analysis [area under the curve (AUC) calculation]. The OS and DFS were evaluated using Kaplan-Meier curves with log-rank testing. Multivariate Cox regression analysis was employed to adjust for potential confounding factors and to evaluate the independent risk factors influencing DFS in cervical cancer.

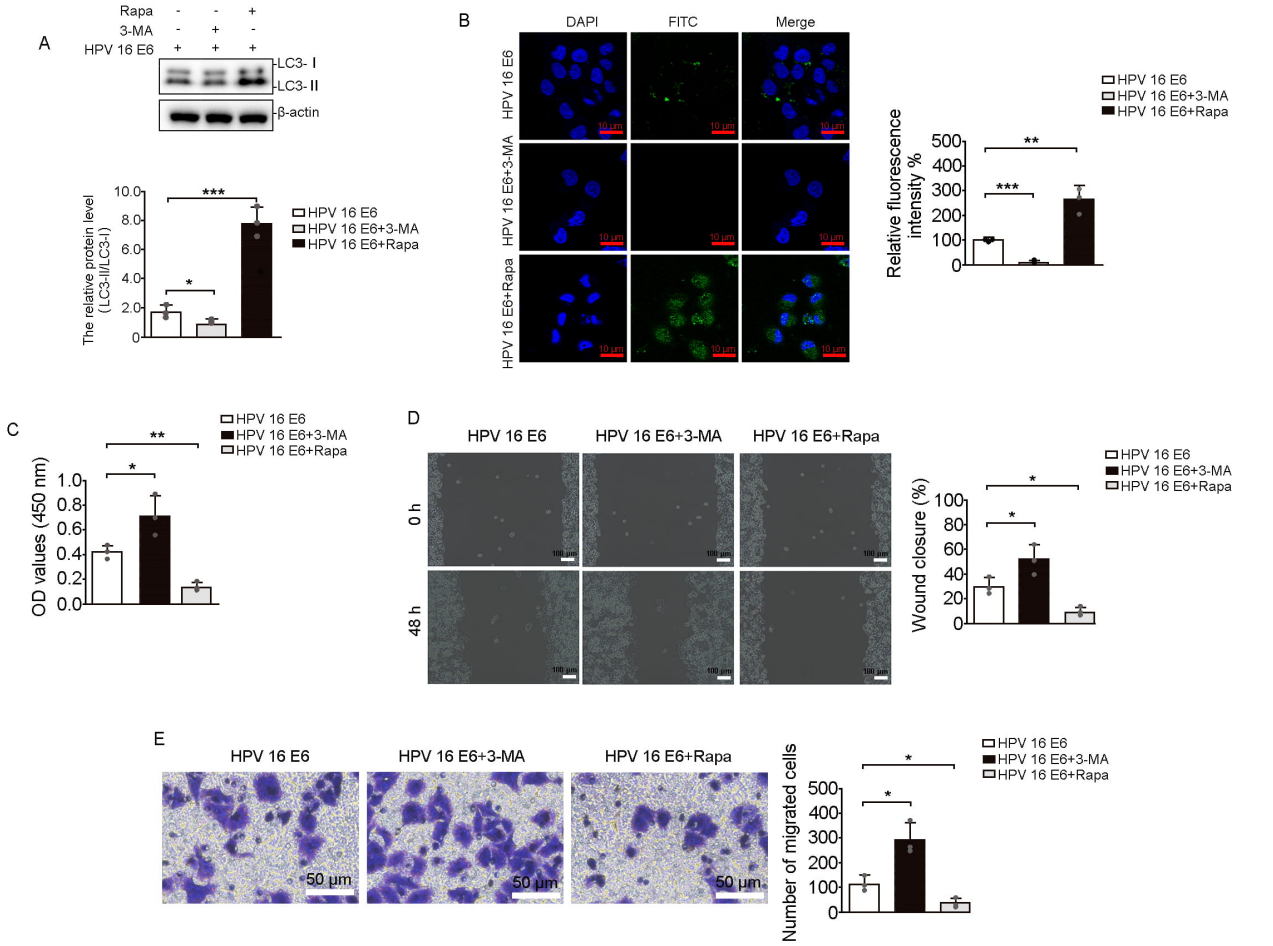

Fig. 1. Role of autophagy in regulating malignant phenotypes in HPV 16 E6-induced C33a cells. C33a cells were transfected with HPV 16 E6 for 48 h, followed by treatment with 3-MA (10 mM) or Rapa (3 μM) for 6 h. (A) Representative immunoblots of LC3 protein levels are presented, with β-actin serving as the loading control. Values represent mean ± SD; $n = 3$ (***$p < 0.001$, *$p < 0.05$ vs. HPV 16 E6 group). (B) Subcellular localization of LC3 (green) was observed by confocal microscopy. Nuclei were stained with DAPI (blue). Scale bars: 10 μm. $n = 3$ (***$p < 0.001$, **$p < 0.01$ vs. HPV 16 E6 group). (C) Cell viability was measured by CCK-8 assay. Values represent mean ± SD; $n = 3$ (**$p < 0.01$, *$p < 0.05$ vs. HPV 16 E6 group). (D,E) Cell migration and invasion abilities were evaluated by wound healing assay and Transwell assay, respectively. Data are presented as mean ± SD; $n = 3$ (*$p < 0.05$ vs. HPV 16 E6 group). HPV, human papillomavirus; 3-MA, 3-methyladenine; Rapa, rapamycin; LC3, microtubule-associated protein 1A/1B-light chain 3; DAPI, 4′,6-diamidino-2-phenylindole; CCK-8, Cell Counting Kit-8; SD, standard deviation.

Multiple comparisons were adjusted using the Bonferroni correction method. The association between CXCL8 and established tumor markers—squamous cell carcinoma antigen (SCC-Ag) and cytokeratin 19 fragment (CYFRA21-1)—was assessed through Pearson's correlation analysis. All analyses were performed using IBM SPSS Statistics for Windows, Version 20.0 (IBM Corp., NY, USA), with statistical significance set at $p < 0.05$ (two-tailed).

Results

The Regulatory Role of Autophagy in the Malignant Progression of HPV 16 E6-Treated C33a Cells

To establish a functional link between autophagy and hrHPV oncogenesis, we evaluated the impact of HPV 16 E6 on LC3 expression in C33a cervical cells. Fig. 1A demonstrates that LC3-II expression was differentially regulated by autophagy modulators: suppressed with 3-MA cotreatment but enhanced with Rapa cotreatment relative to HPV 16 E6 alone ($p < 0.05$ and $p < 0.001$, respectively). Consistent with these findings, cytoplasmic LC3 puncta were abundant in HPV 16 E6 + Rapa treated cells but scarcely detectable in HPV 16 E6 + 3-MA groups (Fig. 1B, $p < 0.01$ and $p < 0.001$, respectively). The CCK-8 assay revealed that the HPV 16 E6 and 3-MA co-treatment significantly increased whereas HPV 16 E6 and Rapa co-treatment significantly decreased the viability of C33a cells compared with HPV 16 E6 alone (Fig. 1C, $p < 0.05$ and $p < 0.01$, respectively). As evidenced by scratch wound healing and Transwell assays, the pro-migratory and pro-invasive activ-

ity induced by HPV 16 E6 was significantly counteracted by Rapa, but was further enhanced by 3-MA (Fig. 1D,E, all $p < 0.05$).

Autophagy Regulated Malignant Phenotypes in C33a Cells via CXCL8

Consistent with our initial speculation, chemokines play a crucial role in autophagy-associated malignant characteristics in cervical cancer. Based on this premise, we systematically evaluated chemokines in C33a cells, focusing on *CXCL10*, *CXCL12*, *CXCL5*, *CXCL1*, *CXCL8*, *CXCL16*, *CCL19*, *CXCL2*, *CXCL4*, and *CCL5*. RT-qPCR analysis revealed that CXCL8 expression was consistently modulated by autophagy levels: the autophagy inducer Rapa significantly downregulated CXCL8 mRNA expression, whereas the inhibitor 3-MA markedly upregulated it. In contrast, although the expression changes in CCL19, CXCL2, and CCL5 reached statistical significance, their responses to autophagy interventions lacked a consistent trend, failing to establish a clear relationship (Fig. 2A, $p < 0.001$, $p < 0.01$ and $p < 0.05$, respectively). Subsequent Western blot and ELISA analyses further confirmed corresponding changes in CXCL8 protein expression and secretion across experimental groups. Notably, Rapa treatment markedly suppressed CXCL8 expression at both the cellular level and in culture supernatants of C33a cells. In contrast, 3-MA treatment exerted an opposing effect, upregulating CXCL8 production (Fig. 2B,C, $p < 0.01$ and $p < 0.05$, respectively). Functional analyses further revealed that concurrent treatment with Rapa and pc-CXCL8 notably enhanced cellular invasiveness and promoted wound closure capacity relative to Rapa and pc-NC co-treatment (Fig. 2D,F, all $p < 0.01$), indicating that CXCL8 overexpression can counteract autophagy activation-mediated suppression of malignant phenotypes. However, 3-MA and anti-CXCL8 co-treatment significantly reduced the number of invasive cells and shortened the cell migration distance compared with the 3-MA alone treatment (Fig. 2E,G, $p < 0.01$ and $p < 0.05$, respectively).

Effect of CXCL8 on the Malignant Phenotypes of HPV 16 E6–Treated C33a Cells

We investigated the role of CXCL8 in hrHPV-induced cervical carcinogenesis by quantifying both intracellular and secreted CXCL8 protein levels. Our data showed that HPV 16 E6 significantly upregulated CXCL8 expression compared to controls ($p < 0.01$). This upregulation was effectively reversed by Rapa co-treatment, which substantially reduced CXCL8 levels relative to HPV 16 E6 alone (Fig. 3A,B; $p < 0.001$ and $p < 0.01$, respectively). Validation experiments confirmed efficient CXCL8 modulation: pc-CXCL8 dramatically increased both CXCL8 mRNA and protein expression when compared with pc-NC group, while anti-CXCL8 antibody treatment effectively suppressed CXCL8 expression compared to control group (**Supplementary Fig. 1**; all $p < 0.01$). Functionally, HPV 16 E6 promoted cell invasion and migration while inhibiting apoptosis. Both Rapa and anti-CXCL8 antibody counteracted these pro-oncogenic effects, significantly decreasing invasive cell numbers and migration distance (Fig. 3C,D; $p < 0.01$, $p < 0.05$, respectively) while simultaneously enhancing apoptosis (Fig. 3E; all $p < 0.01$).

Expression Profile of CXCL8 in Cervical Cancer Specimens

Analysis of CXCL8 expression patterns in cervical cancer tissues revealed distinct clinical associations. Box plot visualization showed significantly higher CXCL8 transcript levels in cervical squamous cell carcinoma and endocervical adenocarcinoma (CESC, $n = 306$) compared to normal tissue controls ($n = 13$, Fig. 4A, $p < 0.05$). However, stage-based comparison demonstrated no statistically significant variation in CXCL8 expression across FIGO stages I-IV [$Pr(>F) = 0.479$, Fig. 4B]. Survival analysis of cervical cancer patients through Kaplan-Meier plotting indicated that high CXCL8 expression significantly correlated with poorer OS (Fig. 4C, log-rank $p = 2.7 \times 10^{-5}$), with a hazard ratio (HR) of 2.81, indicating CXCL8 as a prognostic risk factor (HR >1). Furthermore, IHC assay and RT-qPCR quantification consistently demonstrated enhanced CXCL8 expression in cervical cancer specimens from patients with unfavorable prognosis relative to cases with favorable clinical outcomes (Fig. 4D,E; all $p < 0.01$). This differential expression pattern further supports the association between elevated CXCL8 levels and aggressive disease characteristics. As summarized in Table 1, the chi-square tests identified significant associations between high CXCL8 expression and poor tumor differentiation, cervical infiltration depth $\geq$2/3, and lymph node metastasis ($\chi^2 = 4.235$, 4.675, and 4.461; $p = 0.040$, 0.031, and 0.035, respectively). Additionally, Cox proportional-hazards regression modeling established multiple clinicopathological variables as independent predictors of diminished DFS in cervical cancer. Among these, elevated CXCL8 expression demonstrated the strongest association with affecting DFS (HR = 3.143, 95% confidence interval: 1.519–6.507, $p = 0.002$). Additional significant factors included lymph node metastasis (HR = 2.266), poor tumor differentiation (HR = 2.155), advanced FIGO stage (HR = 2.157), and hrHPV infection (HR = 2.111) (Table 2).

The Prognostic Significance of CXCL8 in Cervical Cancer

To investigate the clinical relevance of CXCL8, patients were dichotomized into high- and low-CXCL8 expression subgroups, and their survival outcomes were evaluated. Patients with lower serum CXCL8 levels exhibited a significantly higher 3-year DFS rate (Fig. 5A, $p < 0.0001$), suggesting a strong association between CXCL8 and cervical cancer outcomes. Correlation assessments with conven-

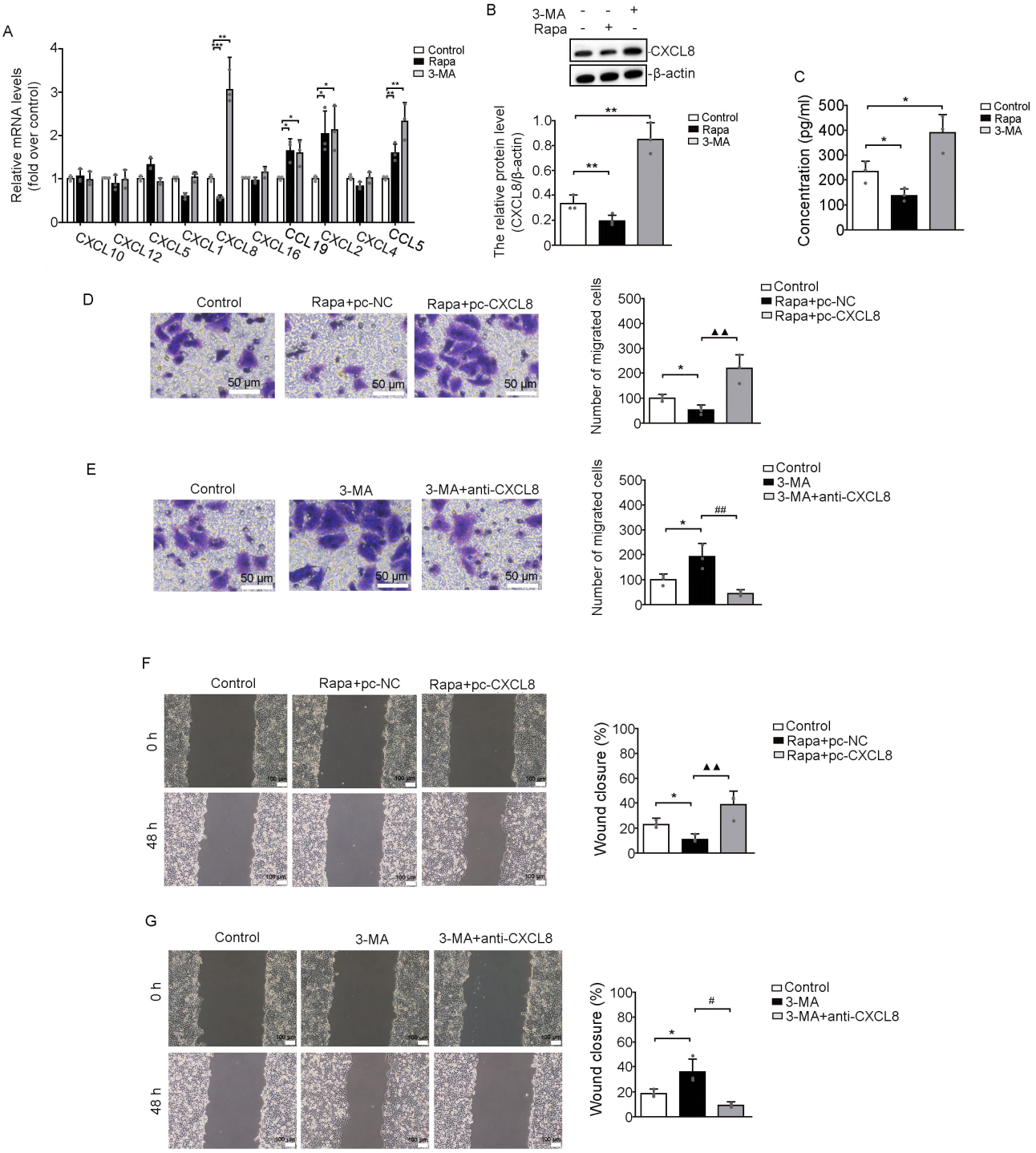

Fig. 2. Autophagy regulated malignant phenotypes in C33a cells via CXCL8. C33a cells were subjected to a 6 h treatment with either 3-MA (10 mM) or Rapa (3 μM). (A) Relative mRNA expression of chemokines in C33a cells was measured by RT-qPCR; n = 3 (***$p < 0.001$, **$p < 0.01$, *$p < 0.05$ vs. control group). (B) CXCL8 protein levels was detected by Western blotting with β-actin as an internal control; n = 3 (**$p < 0.01$ vs. control group). (C) Secreted CXCL8 in culture supernatants was quantified by ELISA; n = 3 (*$p < 0.05$ vs. control group). For functional assays, cells were transfected with pc-NC or pc-CXCL8 (2.5 μg/mL) for 48 h, or treated with anti-CXCL8 antibody (350 ng/mL) for 6 h, followed by 3-MA or Rapa for another 6 h. (D,E) Cell invasion was assessed by Transwell assay. (F,G) Cell migration was evaluated by wound healing assay. n = 3. *$p < 0.05$ vs. control; ▲▲$p < 0.01$ vs. Rapa + pc-NC; ##$p < 0.01$, #$p < 0.05$ vs. 3-MA. CXCL8, C-X-C motif chemokine ligand 8; RT-qPCR, reverse transcription-quantitative PCR; ELISA, enzyme linked immunosorbent assay; pc-NC, an empty pcDNA3.1 vector, serves as a negative control.

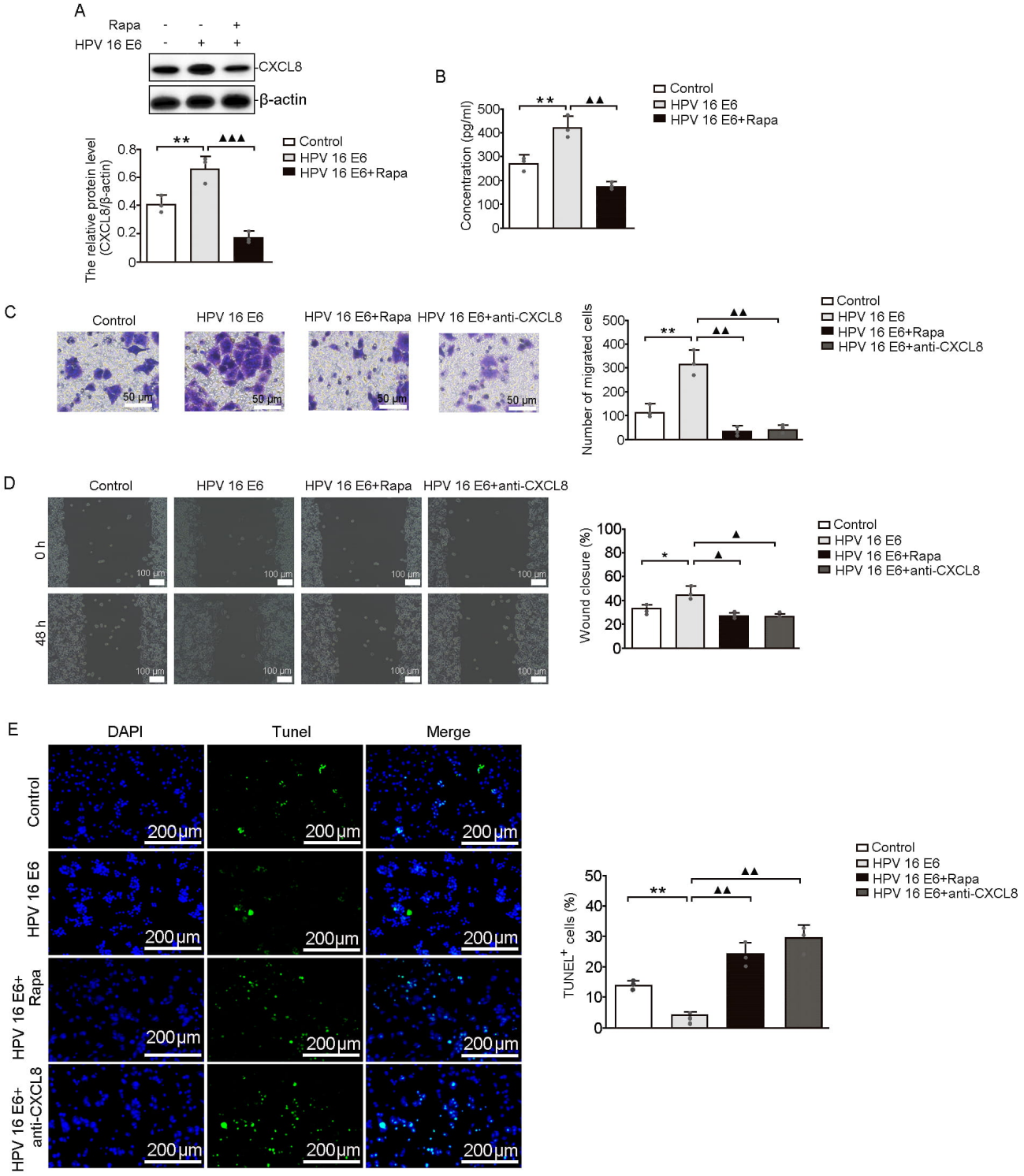

Fig. 3. CXCL8 modulates malignant phenotypes induced by HPV 16 E6 in C33a cells. Prior to a 6 h treatment with either Rapa (3 μM) or an anti-CXCL8 neutralizing antibody (350 ng/mL), C33a cells were transfected with HPV 16 E6 for 48 h. (A) CXCL8 protein expression was analyzed by Western blotting with β-actin serving as a loading control. $n = 3$. $^{**}p < 0.01$ vs. control; $^{▲▲▲}p < 0.001$ vs. HPV 16 E6. (B) Secreted CXCL8 levels in cell culture supernatants were determined by ELISA. $n = 3$. $^{**}p < 0.01$ vs. control; $^{▲▲}p < 0.01$ vs. HPV 16 E6. (C) Cell invasion was evaluated using a Transwell chamber assay. $n = 3$. $^{**}p < 0.01$ vs. control; $^{▲▲}p < 0.01$ vs. HPV 16 E6. (D) Cell migration was measured by wound healing assay. $n = 3$. $^{*}p < 0.05$ vs. control; $^{▲}p < 0.05$ vs. HPV 16 E6. (E) Analysis of apoptosis was conducted with TUNEL assay. $n = 3$. $^{**}p < 0.01$ vs. control; $^{▲▲}p < 0.01$ vs. HPV 16 E6. TUNEL, terminal deoxynucleotidyl transferase–mediated deoxyuridine triphosphate nick-end labeling.

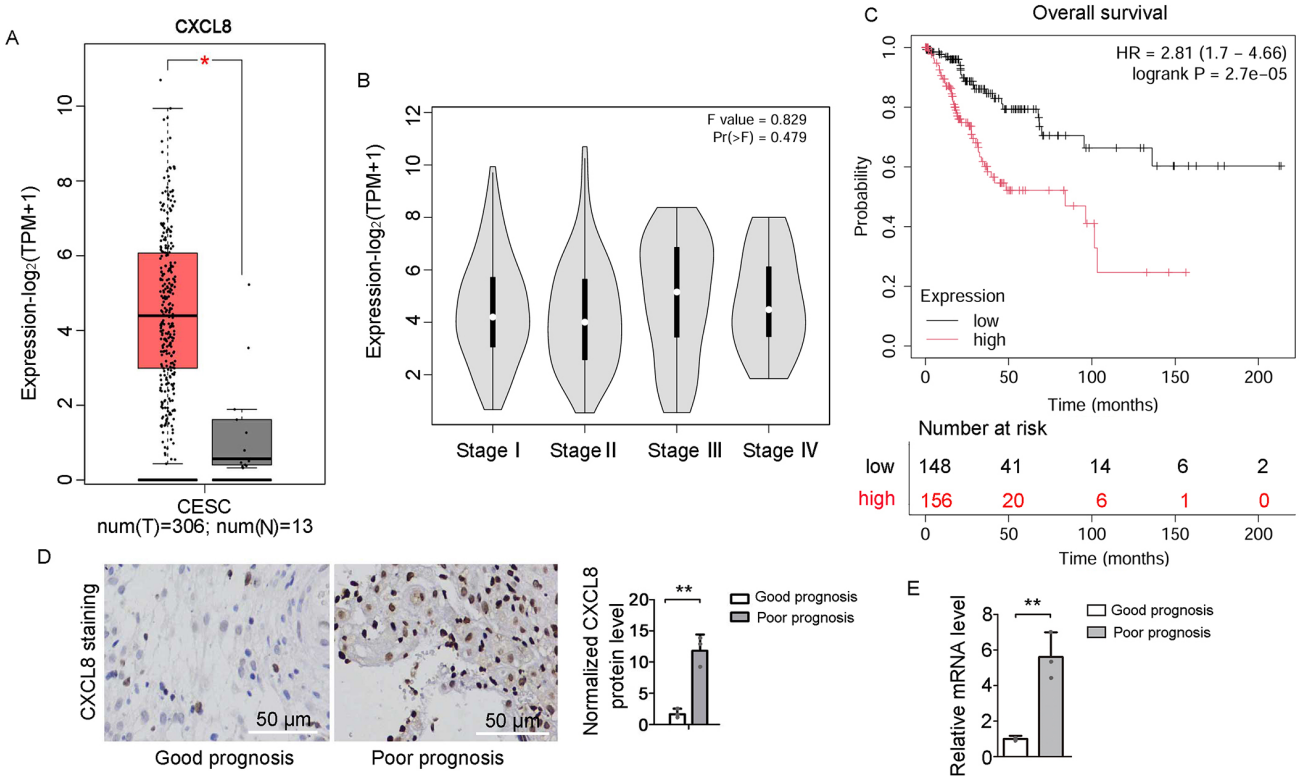

Fig. 4. CXCL8 expression characteristics in cervical cancer tissues. (A) Box plots display the distribution of CXCL8 mRNA expression in 306 CESC specimens (T) and 13 normal controls (N) from the Genotype-Tissue Expression database, presented as box plots. *$p < 0.05$ vs. N group. (B) The stage plot depicts the expression level of *CXCL8* gene across different pathological stages (I–IV) of CESC. A one-way ANOVA was performed to assess the overall difference in its expression among the stages (*Pr(>F)* = 0.479). (C) Kaplan-Meier curves illustrate survival outcomes for 304 cervical cancer cases categorized by high versus low CXCL8 expression levels, with statistical significance determined by the log-rank test ($p = 2.7 \times 10^{-5}$). (D) Representative immunohistochemical images show differential CXCL8 protein expression in tumor specimens from patients with favorable versus poor clinical outcomes (brown = positive staining; scale bars = 50 μm, **$p < 0.01$ vs. good prognosis group). (E) RT-qPCR analysis demonstrates significantly elevated CXCL8 transcript levels in patients with poor clinical outcomes compared to the good-prognosis group. $n = 3$ (**$p < 0.01$ vs. good prognosis group). CESC, cervical squamous cell carcinoma and endocervical adenocarcinoma; ANOVA, Analysis of Variance.

Table 2. Cox regression analysis of factors affecting DFS in patients with cervical cancer.

Variable	Univariate analysis		Multivariate analysis	
	HR (95% CI)	*p*	*HR (95% CI)*	*p*
Age (≥50 years *vs.* <50 years)	1.640 (0.822∼3.274)	0.161	-	-
Tumor diameter (>4 cm *vs.* ≤4 cm)	1.580 (0.806∼3.099)	0.183	-	-
Lymph node metastases (Yes *vs.* No)	2.503 (1.259∼4.977)	0.009	2.266 (1.131∼4.541)	0.021
Cervical infiltration depth (≥2/3 *vs.* <2/3)	2.333 (1.124∼4.842)	0.023	1.094 (0.562∼2.130)	0.791
Differentiation (Low *vs.* Medium/high)	2.612 (1.274∼5.354)	0.009	2.155 (1.086∼4.276)	0.028
FIGO staging (III *vs.* I∼II)	2.525 (1.242∼5.132)	0.010	2.157 (1.076∼4.322)	0.030
hrHPV (Positive *vs.* Negative)	2.573 (1.275∼5.191)	0.008	2.111 (1.046∼4.261)	0.037
CXCL8 (High *vs.* Low)	2.744 (1.339∼5.625)	0.006	3.143 (1.519∼6.507)	0.002

DFS, disease-free survival; HR, hazard ratio; CI, confidence interval; CXCL8, C-X-C motif chemokine ligand 8; hrHPV, high-risk human papillomavirus; FIGO, International Federation of Gynecology and Obstetrics.

tional tumor markers identified strong positive associations of CXCL8 with both SCC-Ag and CYFRA21-1 (Fig. 5B, $r = 0.659$ and 0.499, respectively, all $p < 0.001$). ROC analysis confirmed the prognostic capacity of these markers individually, with AUC values of 0.682 for SCC-Ag, 0.651 for CYFRA21-1, and 0.700 for CXCL8. Notably, a tripartite panel integrating all three biomarkers achieved superior prognostic performance, attaining an AUC of 0.897

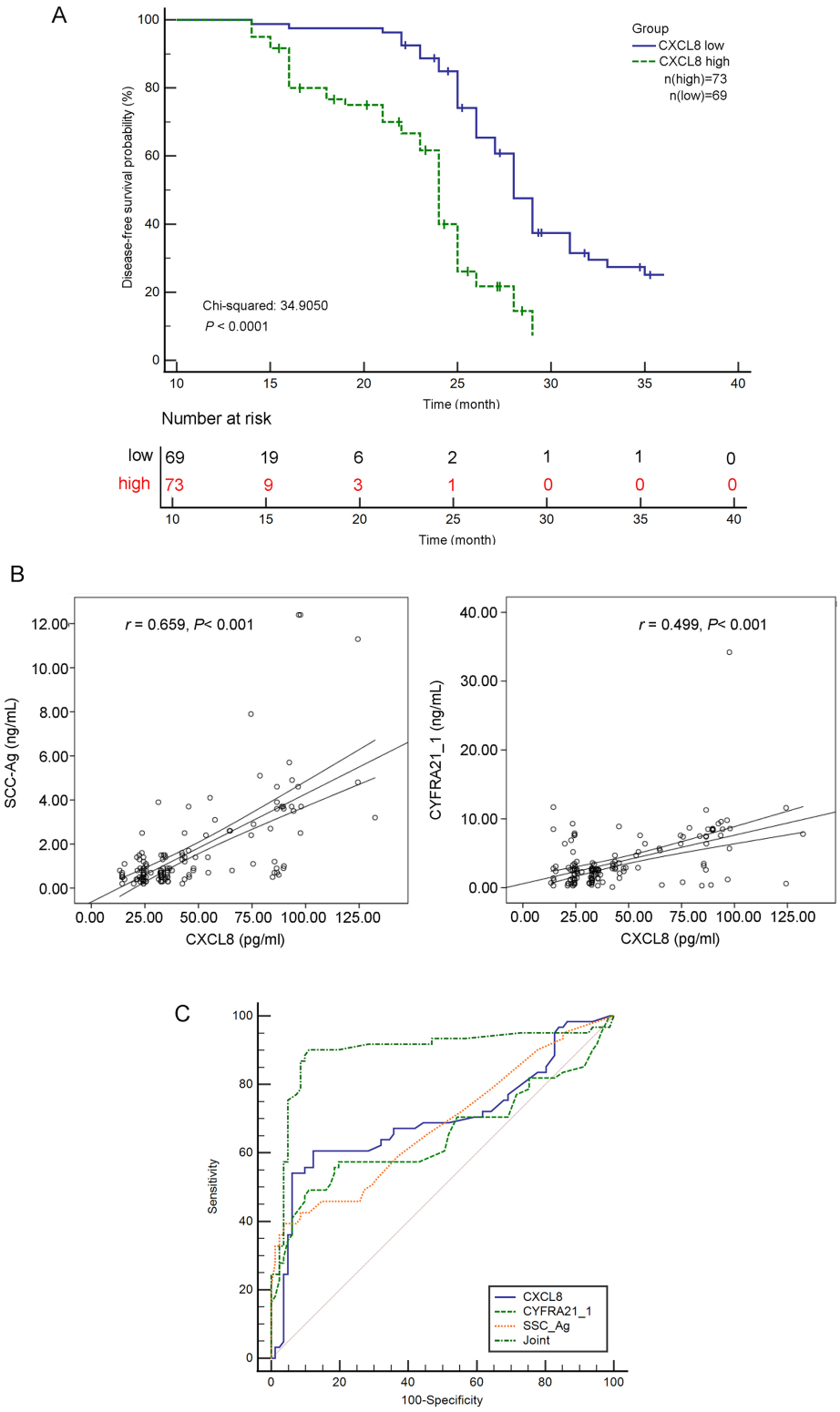

Fig. 5. The prognostic significance of CXCL8 in cervical cancer. (A) Kaplan-Meier curves illustrate DFS outcomes in cervical cancer patients categorized according to high versus low CXCL8 expression levels. $p < 0.0001$. The X-axis is labeled at 5-month intervals for clarity. Survival analysis was based on individual precise survival times. (B) Correlation analysis of CXCL8 with established tumor markers (SCC-Ag and CYFRA21-1). $r = 0.659$ and 0.499, respectively, all $p < 0.001$. (C) ROC curve analysis was performed to assess the prognostic discrimination capacity of SCC-Ag, CYFRA21-1, and CXCL8 between patients with a favorable versus an unfavorable prognosis. DFS, disease-free survival; SCC-Ag, squamous cell carcinoma antigen; CYFRA21-1, cytokeratin 19 fragment; ROC, receiver operating characteristic.

Table 3. The value of SCC-Ag, CYFRA21_1 and CXCL8 in evaluating cervical cancer prognosis.

Variable	AUC	Cut-off	*95% CI*	Youden index	Sensitivity (%)	Specificity (%)
SCC-Ag	0.682	>2.5	0.599∼0.758	0.3564	39.34	96.30
CYFRA21_1	0.651	>4.7	0.566∼0.729	0.3807	49.18	88.89
CXCL8	0.700	>43.6	0.618∼0.774	0.4831	60.66	87.65
Joint	0.897	-	0.835∼0.942	0.7905	90.16	88.89

AUC, area under the curve; CI, confidence interval; CXCL8, C-X-C motif chemokine ligand 8; SCC-Ag, squamous cell carcinoma antigen; CYFRA21-1, cytokeratin 19 fragment.

(95% CI: 0.835–0.942) with 90.16% sensitivity and 88.89% specificity (Fig. 5C, Table 3). DeLong test results indicated no significant difference between the AUC of CXCL8 alone and that of SCC-Ag ($p = 0.6617$) or CYFRA21-1 ($p = 0.3738$). In contrast, the three-biomarker panel showed significantly superior predictive power compared to any single biomarker (**Supplementary Fig. 2**, $p = 0.0009$, 0.0001, and <0.0001, respectively).

Discussion

The association between hrHPV infection and the development of cervical cancer is widely acknowledged; nevertheless, its prognostic relevance in surgically treated cervical cancer patients remains a subject of debate. Multiple studies have demonstrated that hrHPV status may correlate with improved or poorer survival, or may lack any significant prognostic value. For example, HPV 16 positivity has been linked to an unfavorable prognosis, including higher rates of pelvic lymph node metastasis and lymphovascular space invasion, while HPV 18 positivity has been associated with increased mortality and recurrence [26]. Conversely, a large-scale investigation [27] revealed that co-infection with α-7 species (which includes HPV 18) and α-9 species (which includes HPV 16) was correlated with better survival outcomes compared to infection with α-7 species alone, with HPV-negative cases demonstrating the poorest prognosis. In contrast, Zampronha Rde *et al*. [28] observed no significant relationship between hrHPV status and clinical outcomes in cervical cancer patients. Our multivariable Cox regression established hrHPV infection as a driver of disease progression, substantiating its role as an independent prognostic determinant for cervical cancer (HR = 2.111). Thus, further clinical and experimental studies are warranted to clarify the mechanistic role of hrHPV in cervical carcinogenesis.

Our findings establish a critical role for the autophagy pathway in mediating the oncogenic functions of the HPV 16 E6 protein in cervical cancer cells. Specifically, we demonstrate that autophagy is involved in regulating key malignant phenotypes, including cell viability, invasion, and migration. This aligns with the known capacity of oncogenic viruses to co-opt host cellular pathways like autophagy, which can exert dual functions in infection and cancer [29,30]. While it is established that HPV manipulates autophagic processes to facilitate its replication and evade degradation [31,32], our work provides further experimental evidence directly linking this pathway to HPV-driven tumor progression. The value of our research lies in delineating a specific mechanism by which HPV 16 E6 leverages the autophagic machinery to promote cervical cancer aggressiveness. This not only deepens our understanding of viral carcinogenesis but also highlights the autophagy pathway as a potential therapeutic target for counteracting HPV-induced malignancy. However, a key problem that remains is the incomplete understanding of the precise molecular switches that determine whether autophagy acts in a tumor-suppressive or tumor-promotional capacity in different stages of HPV-associated cancer.

Autophagy plays a dual role in cancer that parallels its function in viral infections: depending on the tumor stage and cellular metabolic state, it can either suppress or promote cancer development [33]. While autophagy enhances the invasiveness and therapy resistance of established tumors [34], studies have clearly demonstrated its capacity to prevent tumor formation by maintaining genomic stability [35]. Our experimental data provide direct support for this concept by revealing how the HPV 16 E6 oncoprotein harnesses the autophagy mechanism to escalate the malignancy of cervical cancer cells. This finding aligns with research on mitogen-activated protein kinase kinase kinase kinase 4 (MAP4K4)-induced chemoresistance through the autophagy pathway [36], while also offering a mechanistic explanation for the inverse correlation observed between signal transducer and activator of transcription 3 (STAT3) and autophagic activity in certain contexts [37]. The key breakthrough of our study lies in identifying autophagy as the critical pathway through which the HPV 16 E6 oncoprotein operates. This not only explains why certain HPV infections lead to more aggressive clinical manifestations but also points to new therapeutic directions—suggesting the autophagy machinery as a promising therapeutic target.

Cytokines and chemokines play pivotal roles in malignant tumor progression through their regulation of autophagy [38]. Specifically, CXCL8 can effectively disrupt the dormant state of ovarian cancer cells by suppressing the DIRAS family GTPase 3-mediated autophagy pathway [39]. Furthermore, extracellular vesicles derived from stromal cells enhance radioresistance in prostate cancer cells by delivering CXCL8 to modulate autophagic activ-

ity [40]. Our study employed an integrated approach combining mechanistic investigation and clinical validation to systematically elucidate the pivotal role of the CXCL8-autophagy axis in cervical cancer progression. At the mechanistic level, we demonstrated that the CXCL8-mediated autophagy pathway directly regulates the invasive and migratory capacities of cervical cancer cells, and discovered that CXCL8 blockade effectively reverses the promotion of malignant phenotypes by the HPV 16 E6 oncoprotein via the autophagy pathway. In clinical validation, CXCL8 overexpression showed significant correlations with multiple poor prognostic indicators, including poor tumor differentiation, deep stromal invasion ($\geq$2/3), and lymph node metastasis. Notably, CXCL8 demonstrated a significant synergistic effect when combined with conventional biomarkers (SCC-Ag and CYFRA21-1), suggesting that a composite biomarker panel incorporating CXCL8 could substantially enhance prognostic stratification. The triple-marker panel demonstrated excellent predictive performance (AUC = 0.897, 95% CI: 0.835–0.942; sensitivity 90.16%, specificity 88.89%). Survival analysis further confirmed that high CXCL8 expression was a significant predictor of shorter DFS, independent of clinical stage. These findings not only deepen the understanding of chemokine-regulated autophagy mechanisms but also provide a novel biomarker combination strategy for prognostic assessment in cervical cancer.

It should be noted that this study has certain limitations. First, while the single-center retrospective cohort design provided an initial exploratory foundation, the generalizability of the findings is constrained and requires further validation through multicenter, prospective studies. Second, the current evaluation framework for the predictive model could be further strengthened—for instance, by incorporating more rigorous performance validation methods such as decision curve analysis and calibration curves to comprehensively assess its clinical utility and reliability. To address these limitations, future work will focus on the following directions: ① promoting multicenter clinical collaborative validation to clarify the applicability of the model across diverse populations and healthcare settings; ② establishing a more robust model evaluation framework that integrates multiple validation approaches to continuously optimize predictive performance; and ③ utilizing standardized disease models, such as organoids and animal models, to elucidate the molecular mechanisms of the CXCL8-autophagy regulatory axis in cervical cancer progression and systematically evaluate its potential as a diagnostic and therapeutic target.

Conclusion

This study confirms that CXCL8 serves as a novel prognostic biomarker for hrHPV-associated cervical cancer, with its expression level closely linked to tumor autophagy regulation and clinical progression. By integrating bioinformatic analysis with experimental validation, we have systematically elucidated the regulatory role of CXCL8 in the tumor microenvironment and revealed its potential regulatory network with the HPV 16 E6 oncoprotein. These findings not only provide new insights into the pathogenesis of cervical cancer but also lay a theoretical foundation for developing CXCL8-targeted precision diagnosis and treatment strategies, which may facilitate the clinical translation of individualized therapy for cervical cancer.

Availability of Data and Materials

The datasets generated during and/or analysed during the current study are available from the corresponding author on reasonable request.

Author Contributions

YC made substantial contributions to the conception and design of the study. HYL and LS performed the research and analyzed the data. The first draft of the manuscript was written by YL, who also performed the acquisition, analysis, and interpretation of data. All authors have been involved in revising the manuscript critically for important intellectual content. All authors gave final approval of the version to be published. All authors have participated sufficiently in the work to take public responsibility for appropriate portions of the content and agreed to be accountable for all aspects of the work in ensuring that questions related to its accuracy or integrity.

Ethics Approval and Consent to Participate

This study was performed in line with the principles of the Declaration of Helsinki. Approval was granted by the Medical Ethics Committee of Hongqi Hospital Affiliated to Mudanjiang Medical University (No. 202028). Informed consent was obtained from all individual participants included in the study.

Acknowledgment

Not applicable.

Funding

This study was supported by grants from the Research Projects funded by the Basic Research Business Expenses of Provincial Higher Education Institutions in Heilongjiang Province in 2023 (Contract grant number: 2023-KYYWF-0927).

Conflict of Interest

The authors declare no conflict of interest.

Supplementary Material

Supplementary material associated with this article can be found, in the online version, at https://doi.org/10.24976/Discov.Med.202638205.38.

References

[1] Bray F, Laversanne M, Sung H, Ferlay J, Siegel RL, Soerjomataram I, *et al*. Global cancer statistics 2022: GLOBOCAN estimates of incidence and mortality worldwide for 36 cancers in 185 countries. CA: A Cancer Journal for Clinicians. 2024; 74: 229–263. https://doi.org/10.3322/caac.21834.

[2] Taarnhøj GA, Christensen IJ, Lajer H, Fuglsang K, Jeppesen MM, Kahr HS, *et al*. Risk of recurrence, prognosis, and follow-up for Danish women with cervical cancer in 2005-2013: A national cohort study. Cancer. 2018; 124: 943–951. https://doi.org/10.1002/cncr.31165.

[3] Cao L, Kong W, Li J, Song D, Jin B, Liu T, *et al*. Analysis of Lymph Node Metastasis and Risk Factors in 975 Patients with FIGO 2009 Stage IA-IIA Cervical Cancer. Gynecologic and Obstetric Investigation. 2023; 88: 30–36. https://doi.org/10.1159/000527712.

[4] Ma B, Ren C, Yin Y, Zhao S, Li J, Yang H. Immune cell infiltration and prognostic index in cervical cancer: insights from metabolism-related differential genes. Frontiers in Immunology. 2024; 15: 1411132. https://doi.org/10.3389/fimmu.2024.1411132.

[5] Ma X, Zheng J, He K, Wang L, Wang Z, Wang K, *et al*. TGFA expression is associated with poor prognosis and promotes the development of cervical cancer. Journal of Cellular and Molecular Medicine. 2024; 28: e18086. https://doi.org/10.1111/jcmm.18086.

[6] Vescovo T, Pagni B, Piacentini M, Fimia GM, Antonioli M. Regulation of Autophagy in Cells Infected With Oncogenic Human Viruses and Its Impact on Cancer Development. Frontiers in Cell and Developmental Biology. 2020; 8: 47. https://doi.org/10.3389/fcell.2020.00047.

[7] Aranda-Rivera AK, Cruz-Gregorio A, Briones-Herrera A, Pedraza-Chaverri J. Regulation of autophagy by high- and low-risk human papillomaviruses. Reviews in Medical Virology. 2021; 31: e2169. https://doi.org/10.1002/rmv.2169.

[8] Albano C, Biolatti M, Mazibrada J, Pasquero S, Gugliesi F, Lo Cigno I, *et al*. PAD-mediated citrullination is a novel candidate diagnostic marker and druggable target for HPV-associated cervical cancer. Frontiers in Cellular and Infection Microbiology. 2024; 14: 1359367. https://doi.org/10.3389/fcimb.2024.1359367.

[9] Pi R, Li T, Zhang H, Zhou H, Yang Y, Dai Y, *et al*. The Distribution of HR-HPV E6/E7 DNA and mRNA by Histological Grade and the Clinical Performance for Detection of Cervical Cancer and Precancer. Journal of Medical Virology. 2024; 96: e70026. https://doi.org/10.1002/jmv.70026.

[10] Liu Q, Chen L, Yu M, Zhou X, Zhang X, Zheng W, *et al*. Prevalence of cervical precancers or cancers in women with ASC-H/HSIL cytology according to Aptima HPV (AHPV) assay-detected HPV genotypes and age. Journal of Cancer. 2024; 15: 140–148. https://doi.org/10.7150/jca.89715.

[11] Ruiz FJ, Inkman M, Rashmi R, Muhammad N, Gabriel N, Miller CA, *et al*. HPV transcript expression affects cervical cancer response to chemoradiation. JCI Insight. 2021; 6: e138734. https://doi.org/10.1172/jci.insight.138734.

[12] Liu J, Wu Y, Meng S, Xu P, Li S, Li Y, *et al*. Selective autophagy in cancer: mechanisms, therapeutic implications, and future perspectives. Molecular Cancer. 2024; 23: 22. https://doi.org/10.1186/s12943-024-01934-y.

[13] Akram N, Imran M, Noreen M, Ahmed F, Atif M, Fatima Z, *et al*. Oncogenic Role of Tumor Viruses in Humans. Viral Immunology. 2017; 30: 20–27. https://doi.org/10.1089/vim.2016.0109.

[14] Damian D. The Role of Viruses in Cellular Transformation and Cancer. Cancer Reports (Hoboken, N.J.). 2025; 8: e70150. https://doi.org/10.1002/cnr2.70150.

[15] Zhang Y, Ma Y, Zhao C, Zhang H, Pu Y, Yin L. Synergistic Carcinogenesis of HPV18 and MNNG in Het-1A Cells through p62-KEAP1-NRF2 and PI3K/AKT/mTOR Pathway. Oxidative Medicine and Cellular Longevity. 2020; 2020: 6352876. https://doi.org/10.1155/2020/6352876.

[16] Zhou X, Münger K. Expression of the human papillomavirus type 16 E7 oncoprotein induces an autophagy-related process and sensitizes normal human keratinocytes to cell death in response to growth factor deprivation. Virology. 2009; 385: 192–197. https://doi.org/10.1016/j.virol.2008.12.003.

[17] Antonioli M, Pagni B, Vescovo T, Ellis R, Cosway B, Rollo F, *et al*. HPV sensitizes OPSCC cells to cisplatin-induced apoptosis by inhibiting autophagy through E7-mediated degradation of AMBRA1. Autophagy. 2021; 17: 2842–2855. https://doi.org/10.1080/15548627.2020.1847444.

[18] Thongchot S, Jamjuntra P, Therasakvichya S, Warnnissorn M, Ferraresi A, Thuwajit P, *et al*. Interleukin 8 released by cancer associated fibroblasts attenuates the autophagy and promotes the migration of ovarian cancer cells. International Journal of Oncology. 2021; 58: 14. https://doi.org/10.3892/ijo.2021.5194.

[19] Abu-Rustum NR, Campos SM, Amarnath S, Arend R, Barber E, Bradley K, *et al*. NCCN Guidelines Insights: Uterine Neoplasms, Version 3.2025. Journal of the National Comprehensive Cancer Network. 2025; 23: 284–291. https://doi.org/10.6004/jnccn.2025.0038.

[20] Zhou H, Liu YY, Yu XL, Lin ZQ. Interpretation of "2025 NCCN Clinical Practice Guidelines in Oncology: Cervical Cancer (Version 1.0)". Chinese Journal of Practical Gynecology and Obstetrics. 2025; 41: 96–102. https://doi.org/10.19538/j.fk2025010122. (In Chinese)

[21] Bhatla N, Berek JS, Cuello Fredes M, Denny LA, Grenman S, Karunaratne K, *et al*. Revised FIGO staging for carcinoma of the cervix uteri. International Journal of Gynaecology and Obstetrics: the Official Organ of the International Federation of Gynaecology and Obstetrics. 2019; 145: 129–135. https://doi.org/10.1002/ijgo.12749.

[22] Cen S, Wang P, Xie Z, Yang R, Li J, Liu Z, *et al*. Autophagy enhances mesenchymal stem cell-mediated $CD4^+$ T cell migration and differentiation through CXCL8 and TGF-β1. Stem Cell Research & Therapy. 2019; 10: 265. https://doi.org/10.1186/s13287-019-1380-0.

[23] Livak KJ, Schmittgen TD. Analysis of relative gene expression data using real-time quantitative PCR and the 2(-Delta Delta C(T)) Method. Methods (San Diego, Calif.). 2001; 25: 402–408. https://doi.org/10.1006/meth.2001.1262.

[24] Martinho O, Pinto F, Granja S, Miranda-Gonçalves V, Moreira MAR, Ribeiro LFJ, *et al*. RKIP inhibition in cervical cancer is associated with higher tumor aggressive behavior and resistance to cisplatin therapy. PloS One. 2013; 8: e59104. https://doi.org/10.1371/journal.pone.0059104.

[25] Wang W, Gu Y, Ni H, Quan Q, Guo L. Silencing of FAM111B inhibits tumor growth and promotes apoptosis by decreasing AKT activity in ovarian cancer. Experimental Biology and Medicine (Maywood, N.J.). 2023; 248: 1043–1055. https://doi.org/10.1177/15353702231160326.

[26] Aimagambetova G, Bapayeva G, Ukybassova T, Kamzayeva N, Sakhipova G, Shanazarov N, *et al*. Risks of Cervical Cancer Recurrence After Fertility-Sparing Surgery and the Role of Human

Papillomavirus Infection Types. Journal of Clinical Medicine. 2024; 13: 6318. https://doi.org/10.3390/jcm13216318.

[27] Zhao J, Zhan Q, Guo J, Liu M, Ruan Y, Zhu T, *et al*. Phylogeny and polymorphism in the E6 and E7 of human papillomavirus: alpha-9 (HPV 16, 31, 33, 52, 58), alpha-5 (HPV51), alpha-6 (HPV53, 66), alpha-7 (HPV18, 39, 59, 68) and alpha-10 (HPV6, 44) in women from Shanghai. Infectious Agents and Cancer. 2019; 14: 38. https://doi.org/10.1186/s13027-019-0250-9.

[28] Zampronha Rde A, Freitas-Junior R, Murta EFC, Michelin MA, Barbaresco AA, Adad SJ, *et al*. Human papillomavirus types 16 and 18 and the prognosis of patients with stage I cervical cancer. Clinics (Sao Paulo, Brazil). 2013; 68: 809–814. https://doi.org/10.6061/clinics/2013(06)14.

[29] Chen T, Tu S, Ding L, Jin M, Chen H, Zhou H. The role of autophagy in viral infections. Journal of Biomedical Science. 2023; 30: 5. https://doi.org/10.1186/s12929-023-00899-2.

[30] Jin KT, Tao XH, Fan YB, Wang SB. Crosstalk between oncolytic viruses and autophagy in cancer therapy. Biomedicine & Pharmacotherapy = Biomedecine & Pharmacotherapie. 2021; 134: 110932. https://doi.org/10.1016/j.biopha.2020.110932.

[31] Shi Y, Yan S, Shao GC, Wang J, Jian YP, Liu B, *et al*. O-GlcNAcylation stabilizes the autophagy-initiating kinase ULK1 by inhibiting chaperone-mediated autophagy upon HPV infection. The Journal of Biological Chemistry. 2022; 298: 102341. https://doi.org/10.1016/j.jbc.2022.102341.

[32] Liu S, Su Y, Lu Z, Zou X, Xu L, Teng Y, *et al*. The SFTSV Nonstructural Proteins Induce Autophagy to Promote Viral Replication via Interaction with Vimentin. Journal of Virology. 2023; 97: e0030223. https://doi.org/10.1128/jvi.00302-23.

[33] Zahedi-Amiri A, Malone K, Beug ST, Alain T, Yeganeh B. Autophagy in Tumor Immunity and Viral-Based Immunotherapeutic Approaches in Cancer. Cells. 2021; 10: 2672. https://doi.org/10.3390/cells10102672.

[34] Niu X, You Q, Hou K, Tian Y, Wei P, Zhu Y, *et al*. Autophagy in cancer development, immune evasion, and drug resistance. Drug Resistance Updates: Reviews and Commentaries in Antimicrobial and Anticancer Chemotherapy. 2025; 78: 101170. https://doi.org/10.1016/j.drup.2024.101170.

[35] Vessoni AT, Filippi-Chiela EC, Menck CF, Lenz G. Autophagy and genomic integrity. Cell Death and Differentiation. 2013; 20: 1444–1454. https://doi.org/10.1038/cdd.2013.103.

[36] Huang H, Han Q, Zheng H, Liu M, Shi S, Zhang T, *et al*. MAP4K4 mediates the SOX6-induced autophagy and reduces the chemosensitivity of cervical cancer. Cell Death & Disease. 2021; 13: 13. https://doi.org/10.1038/s41419-021-04474-1.

[37] Wu L, Shen B, Li J, Zhang H, Zhang K, Yang Y, *et al*. STAT3 exerts pro-tumor and anti-autophagy roles in cervical cancer. Diagnostic Pathology. 2022; 17: 13. https://doi.org/10.1186/s13000-021-01182-4.

[38] Hu F, Song D, Yan Y, Huang C, Shen C, Lan J, *et al*. IL-6 regulates autophagy and chemotherapy resistance by promoting BECN1 phosphorylation. Nature Communications. 2021; 12: 3651. https://doi.org/10.1038/s41467-021-23923-1.

[39] Mao W, Peters HL, Sutton MN, Orozco AF, Pang L, Yang H, *et al*. The role of vascular endothelial growth factor, interleukin 8, and insulinlike growth factor in sustaining autophagic DIRAS3-induced dormant ovarian cancer xenografts. Cancer. 2019; 125: 1267–1280. https://doi.org/10.1002/cncr.31935.

[40] Wang X, Xu F, Kou H, Zheng Y, Yang J, Xu Z, *et al*. Stromal cell-derived small extracellular vesicles enhance radioresistance of prostate cancer cells via interleukin-8-induced autophagy. Journal of Extracellular Vesicles. 2023; 12: e12342. https://doi.org/10.1002/jev2.12342.